

# Enforcing Analytic Constraints in Neural-Networks Emulating Physical Systems

Tom Beucler,<sup>1,2,\*</sup> Michael Pritchard,<sup>1</sup> Stephan Rasp,<sup>3</sup> Pierre Gentine,<sup>2</sup> and Jordan Ott, Pierre Baldi<sup>4</sup>

<sup>1</sup>*Department of Earth System Science, University of California, Irvine, CA, USA*

<sup>2</sup>*Department of Earth and Environmental Engineering, Columbia University, New York, NY, USA*

<sup>3</sup>*Technical University of Munich, Munich, Germany*

<sup>4</sup>*Department of Computer Science, University of California, Irvine, CA, USA*

(Dated: September 19, 2019)

Neural networks can emulate non-linear physical systems with high accuracy, yet they may produce physically-inconsistent results when violating fundamental constraints. In this letter, we introduce a systematic way of enforcing analytic constraints in neural networks via constraints in the architecture or the loss function. Applied to the modeling of convective processes for climate modeling, architectural constraints can enforce conservation laws to within machine precision without degrading performance. Furthermore, enforcing constraints can reduce the error of variables closely related to the constraints.

Figures and Tables: [https://github.com/tbeucler/CBRAIN-CAM/blob/master/notebooks/tbeucler\\_devlog/022\\_Figure\\_Conserving\\_NN.ipynb](https://github.com/tbeucler/CBRAIN-CAM/blob/master/notebooks/tbeucler_devlog/022_Figure_Conserving_NN.ipynb)

Main Repository: <https://github.com/raspstephan/CBRAIN-CAM>

## I. INTRODUCTION

Many fields of science and engineering (e.g., hydrology, solid mechanics, chemistry kinetics) have exact, often *analytic*, closed-form constraints, i.e. constraints that can be explicitly written using analytic functions of the system's variables. Examples include translational or rotational invariance, conservation laws, or equations of state. While physically-consistent models should enforce constraints to within machine precision, data-driven algorithms often fail to satisfy well-known constraints that are not explicitly enforced. In particular, neural networks (NN), powerful regression tools for non-linear systems, may severely violate constraints on individual samples while optimizing overall performance.

Despite the need for hybrid-NNs to model complex physical systems [1–3], enforcing *hard* constraints [4] has been limited to physical systems governed by specific equations, such as advection [5–7] or Reynolds-averaged Navier-Stokes [8, 9] equations. To address this gap, we introduce a systematic method to enforce analytic constraints arising in more general physical systems to within machine precision (Architecture-constrained NN or ACnet). We then compare ACnet to unconstrained (UCnet) and loss-constrained NN (LCnet, in which soft constraints are added through a penalization term in the loss function [e.g., 10, 11]) in the particular case of climate modeling, where the system is high-dimensional and the constraints are few but crucial [12].

## II. THEORY

### A. Formulating the Constraints

Enforcing constraints is easiest for linearly-constrained NNs, i.e. NNs for which the constraints ( $\mathcal{C}$ ) can be written as a linear system of rank  $n$ :

$$(\mathcal{C}) \stackrel{\text{def}}{=} \left\{ \mathbf{C} \begin{bmatrix} \mathbf{x} \\ \mathbf{y} \end{bmatrix} = \mathbf{0} \right\}. \quad (1)$$

We call  $\mathbf{C} \in \mathbb{R}^n \times \mathbb{R}^{m+p}$  the constraints matrix, where  $\mathbf{x} \in \mathbb{R}^m$  is the input vector, and  $\mathbf{y} \in \mathbb{R}^p$  the output vector. Bold font indicates vectors and tensors to distinguish them from scalars. For the regression problem to have non-unique solutions, the number of independent constraints  $n$  has to be strictly less than  $m + p$ .

In Figure 1, we consider a generic regression problem subject to analytic constraints ( $\mathcal{C}$ ) that may be non-linear, and propose how to formulate a linearly-constrained NN. First, define the regression's inputs  $\mathbf{x}_0$  and outputs  $\mathbf{y}_0$ , which respectively become the *temporary* NN's features and targets. Then, write the constraints ( $\mathcal{C}$ ) as a function  $\mathbf{c}$  of the inputs, the outputs, and additional parameters  $\mathbf{z}$  the constraints may involve.  $\mathbf{c}$  must equal  $\mathbf{0}$ , yielding **Formulation 1**. We recommend non-dimensionalizing all variables to facilitate the design and interpretation of the loss functions. While the function  $\mathbf{c}$  may be non-linear, it can always be written as the sum of: (1) terms *x only* dependent on inputs and (2) terms *y* dependent on inputs, outputs and additional parameters. Thus the constraints can be written as:

$$\mathbf{c}(\mathbf{x}_0, \mathbf{y}_0, \mathbf{z}) = \mathbf{C} \begin{bmatrix} \mathbf{x}(\mathbf{x}_0) \\ \mathbf{y}(\mathbf{x}_0, \mathbf{y}_0, \mathbf{z}) \end{bmatrix}, \quad (2)$$

where  $\mathbf{C}$  is a matrix. Finally, choose  $\mathbf{x}$  and  $\mathbf{y}$  as the NN's new inputs and outputs. If  $\mathbf{x}$  and  $\mathbf{y}$  are not bijective functions, add variables to the NN's inputs and outputs to recover  $\mathbf{x}_0$  and  $\mathbf{y}_0$  after optimization (e.g., we

\* tom.beucler@gmail.com

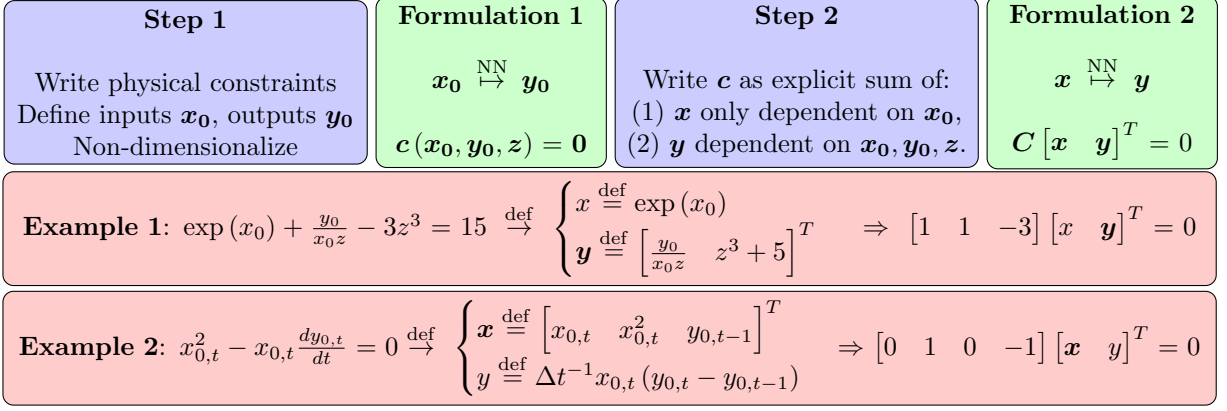


FIG. 1. Framework to treat constrained regression problems using linearly-constrained NNs, with two examples: (1) A regression problem with one non-linear constraint, and (2) a time-prediction problem with one differential non-linear constraint that we discretize using a forward Euler method of timestep  $\Delta t$ . Note that the choice of  $\mathbf{x}$ ,  $\mathbf{y}$ , and  $\mathbf{C}$  is not unique.

add  $x_{0,t}$  and  $y_{0,t-1}$  to  $\mathbf{x}$  in **Example 2**). This yields **Formulation 2**. We are now in a position to build a computationally-efficient NN that satisfies the linear constraints ( $\mathbf{C}$ ).

### B. Enforcing the Constraints

Consider a NN trained on preexisting measurements of  $\mathbf{x}$  and  $\mathbf{y}$ . For simplicity's sake, we measure the quality of its output  $\mathbf{y}_{\text{NN}}$  using a standard mean-squared error (MSE) misfit:

$$\text{MSE}(\mathbf{y}_{\text{Truth}}, \mathbf{y}_{\text{NN}}) \stackrel{\text{def}}{=} \|\mathbf{y}_{\text{Err}}\|_2 \stackrel{\text{def}}{=} \frac{1}{p} \sum_{k=1}^p y_{\text{Err},k}^2, \quad (3)$$

where we have introduced the error vector, defined as the difference between the NN's output and the "truth":

$$\mathbf{y}_{\text{Err}} \stackrel{\text{def}}{=} \mathbf{y}_{\text{NN}} - \mathbf{y}_{\text{Truth}}. \quad (4)$$

In the reference case of an "unconstrained network" (UCnet), we optimize a multi-layer perceptron [e.g., 13, 14] using MSE as its loss function  $\mathcal{L}$ . To enforce the constraints ( $\mathbf{C}$ ) within our NN, we consider two options:

**(1) Constraining the loss function (LCnet, soft constraints):** We penalize the NN for violating physical constraints using a penalty  $\mathcal{P}$ , defined as the mean-squared residual from the constraints:

$$\begin{aligned} \mathcal{P}(\mathbf{x}, \mathbf{y}_{\text{NN}}) &\stackrel{\text{def}}{=} \left\| \mathbf{C} \begin{bmatrix} \mathbf{x} \\ \mathbf{y}_{\text{NN}} \end{bmatrix} \right\|_2, \\ &= \frac{1}{n} \sum_{i=1}^n \left( \sum_{j=1}^m C_{ij} x_j + \sum_{k=1}^p C_{i(k+m)} y_{\text{NN},k} \right)^2, \end{aligned} \quad (5)$$

and treat the constraints as *soft* by giving the penalty  $\mathcal{P}$  a weight  $\alpha \in [0, 1]$  in the loss function  $\mathcal{L}$ :

$$\mathcal{L}(\alpha) = \alpha \mathcal{P}(\mathbf{x}, \mathbf{y}_{\text{NN}}) + (1 - \alpha) \text{MSE}(\mathbf{y}_{\text{Truth}}, \mathbf{y}_{\text{NN}}). \quad (6)$$

**(2) Constraining the architecture (ACnet, hard constraints):** We treat the constraints as *hard* and augment a standard NN with  $n$  conservation layers to enforce the constraints ( $\mathbf{C}$ ) to within machine precision (Figure 2), while keeping the MSE as the loss function:

$$(\text{ACnet}) \Rightarrow \left\{ \min \text{MSE} \text{ s.t. } \mathbf{C} [\mathbf{x} \ \mathbf{y}_{\text{NN}}]^T = \mathbf{0} \right\} \quad (7)$$

The standard NN calculates a "direct" output whose size is  $p-n$ . We then calculate the remaining output's components of size  $n$  as exact "residuals" from the constraints. Concatenating the "direct" and "residual" components results in the full output  $\mathbf{y}_{\text{NN}}$  that satisfies the constraints to within machine precision. Since our loss uses the full output  $\mathbf{y}_{\text{NN}}$ , the gradients of the loss function are passed through the constraints layers during optimization, meaning that the final NN's weights and biases depend on the constraints ( $\mathbf{C}$ ). A possible implementation of the constraints layer uses custom Tensorflow layers of fixed weights that solve the system of equations ( $\mathbf{C}$ ), in row-echelon form, from the bottom to the top row (Appendix B.1). Note that we are free to choose which outputs to calculate as "residuals", which introduces new hyperparameters (Appendix B.2).

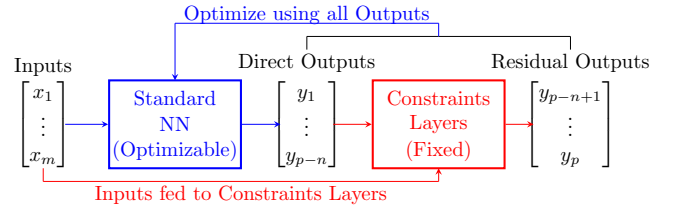


FIG. 2. ACnet: Direct outputs are calculated using a standard NN, while the remaining outputs are calculated as residuals from the fixed constraints layers.

### C. Linking Constraints to Performance

Intuitively, we expect NNs’ performance to improve once we enforce constraints arising in physical systems with few degrees of freedom, but this may not hold true with many degrees of freedom. We formalize the link between constraints and performance by: (1) decomposing the NN’s prediction into the “truth” and error vectors following equation 4, and (2) remembering that constraints exactly hold for the “truth”. This yields:

$$C \begin{bmatrix} \mathbf{x} \\ \mathbf{y}_{\text{NN}} \end{bmatrix} \stackrel{\text{def}}{=} \overbrace{C \begin{bmatrix} \mathbf{x} \\ \mathbf{y}_{\text{Truth}} \end{bmatrix}}^{\mathbf{0}} + C \begin{bmatrix} \mathbf{0} \\ \mathbf{y}_{\text{Err}} \end{bmatrix}. \quad (8)$$

Equation 8 relates how much the constraints are violated to the error vector. More precisely, if we measure performance using the MSE, we may square each component of Equation 8 to relate how much the constraints are violated to the squared error loss and to residual cross terms; for each constraint of index  $i \in \llbracket 1, n \rrbracket$ :

$$\underbrace{\left( C \begin{bmatrix} \mathbf{x} \\ \mathbf{y}_{\text{NN}} \end{bmatrix} \right)_i^2}_{\text{Physical constraints}} = \underbrace{\sum_{k=1}^p C_{i(k+m)}^2 y_{\text{Err},k}^2}_{\text{Squared-error} > 0} + \underbrace{\sum_{k=1}^p \sum_{l \neq k} C_{i(k+m)} C_{i(l+m)} y_{\text{Err},k} y_{\text{Err},l}}_{\text{Cross-term}} \quad (9)$$

In ACnets, we strictly enforce physical constraints, setting the left-hand side of equation 9 to 0. As the squared-error is positive-definite, the cross-term is always negative in ACnets. It is difficult to predict the cross-term before optimization, hence equation 9 does not provide a-priori predictions of performance, even for ACnets. Instead, it links the constraint violation of the NN to the performance of related predictions: the more negative the cross-term, the larger the squared-error for a given violation of physical constraints.

## III. APPLICATION

### A. Convective Parametrization for Climate Modeling

The representation of subgrid-scale processes in coarse-scale, numerical models of the atmosphere, referred to as subgrid *parametrization*, is a large source of error and uncertainty [e.g., 15, 16]. Machine-learning algorithms trained on fine-scale, turbulence-permitting models can improve subgrid parametrizations by faithfully emulating the effect of fine-scale processes on coarse-scale dynamics [e.g., 17–20, see section 2 of Rasp [21] for a detailed review]. The problem is that none of these parametrizations exactly follow conservation laws (e.g., conservation of mass, energy). This is critical for long-term climate projections, as the spurious energy production may both exceed the projected radiative forcing and result in large thermodynamic drifts or biases over a long time-period. Motivated by this shortcoming, we build a NN parametrization of convection and clouds that we *constrain* to conserve 4 quantities: energy, mass, longwave radiation, and shortwave radiation.

### B. Model and Data

We use the Super-Parametrized Community Atmosphere Model 3.0 [22] to simulate the climate for two years in aquaplanet configuration [23], where the surface temperatures are fixed with a realistic equator-to-pole gradient [24]. Following [18]’s sensitivity tests, we work in a *data-rich* regime by using 42M samples from the simulation’s first year to train the NN and 42M samples from the simulation’s second year to validate the NN. To test the NNs’ ability to generalize outside of their training set, we use 42M samples from a simulation in which the surface temperature has been uniformly warmed by 4K, a proxy for the effects of climate change.

### C. Formulating the Conservation Laws in a Neural Network

The parametrization’s goal is to predict the rate at which convection vertically redistributes heat and water based on the climate’s current state. We group all variables describing the local climate in an input vector  $\mathbf{x}$  of size 304 (10 vertical profiles with 30 levels, followed by 4 scalars):

$$\mathbf{x} = \left[ (\mathbf{q}_v, \mathbf{q}_l, \mathbf{q}_i, \mathbf{T}, \mathbf{v}, \mathbf{LS}, p_s, S_0) \text{ SHF LHF} \right]^T, \quad (10)$$

where all variables are defined in Appendix A. We then concatenate the time-tendencies from convection and the additional variables involved in the conservation laws to form an output vector  $\mathbf{y}$  of size 216 (7 vertical profiles with 30 levels, followed by 6 scalars):

$$\mathbf{y} = [\dot{q}_v \ \dot{q}_l \ \dot{q}_i \ \dot{T} \ \dot{T}_{KE} \ \text{lw} \ \text{sw} \ \text{LW}_t \ \text{LW}_s \ \text{SW}_t \ \text{SW}_s \ P \ P_i]^T, \quad (11)$$

We normalize all variables to the same units before non-dimensionalizing them using the constant  $1\text{W m}^{-2}$  (Appendix A.5). Finally, we derive the dimensionless

conservation laws (Appendix A.1-A.4), and write them as a sparse matrix of size  $4 \times (304 + 218)$  that acts on  $\mathbf{x}$  and  $\mathbf{y}$  to yield equation 1:

$$\mathbf{C} = \begin{bmatrix} \mathbf{0} & 1 & \ell_s & -\ell_s \delta p & -\ell_f \delta p & \mathbf{0} & -\delta p & \delta p & \mathbf{0} & \mathbf{0} & -1 & 1 & 1 & -1 & -\ell_f & \ell_f \\ \mathbf{0} & \mathbf{0} & 1 & -\delta p & -\delta p & -\delta p & \mathbf{0} & \mathbf{0} & \mathbf{0} & \mathbf{0} & 0 & 0 & 0 & 0 & -1 & 0 \\ \mathbf{0} & \delta p & \mathbf{0} & 1 & -1 & 0 & 0 & 0 & 0 \\ \mathbf{0} & \delta p & 0 & 0 & -1 & 1 & 0 & 0 \end{bmatrix}, \quad (12)$$

Each row of the conservation matrix  $\mathbf{C}$  describes a different conservation law: The first row is enthalpy conservation (here equivalent to energy conservation), the second row is water conservation (here equivalent to mass conservation), the third row is longwave radiation conservation and the last row is shortwave radiation conservation.

#### D. Implementation

We implement the three NN types (UCnet, LCnet, ACnet) using the Keras library [25] with the Tensorflow backend [26]. In our reference ACnet, we write the constraints layers in Tensorflow to solve the system of equations ( $\mathcal{C}$ ) from bottom to top, and calculate surface tendencies as residuals of the conservation equations (Appendix B.1); switching the “residual” outputs to different vertical levels does not significantly change the validation loss nor the constraints penalty (Appendix B.2). After testing multiple architectures and activation functions (Appendix C.2), we chose 5 hidden layers of 512 nodes with leaky rectified linear-unit activations as our standard multi-layer perceptron architecture. We optimized the NN’s weights and biases with the RMSprop optimizer [27] because it was more stable than the Adam optimizer [28] for LCnets, and save the NN’s state of minimal validation loss over 20 epochs.

#### E. Results

In Figure 3a, we compare mean performance (measured by MSE) and by how much physical constraints are violated (measured by  $\mathcal{P}$ ) for our three NN types: (1) LCnets for which we vary the weight  $\alpha$  given to conservation laws from 0 to 1 (Equation 6), (2) our reference ACnet, and (3) UCnet, i.e. a LCnet of weight  $\alpha = 0$ . As expected, we note a monotonic trade-off between performance and constraints as we increase  $\alpha$  from 0 to 1 in the loss function. Interestingly, the physical constraints

are easier to satisfy than reducing MSE in our case, likely because it is difficult to deterministically predict precipitation, which is strongly non-Gaussian and inherently stochastic. Despite this, UCnet may violate physical constraints more than its multi-linear regression counterpart. Our first key result is that ACnet performs to within  $3\text{W}^2\text{m}^{-4}$  of our lowest-MSE UCnet while satisfying constraints to  $\mathcal{O}(10^{-9}\text{W}^2\text{m}^{-4})$  (Appendix C.1). Tested in “out-of-training” conditions (+4K), ACnet still satisfies constraints to  $\mathcal{O}(10^{-9}\text{W}^2\text{m}^{-4})$ , but performs less well than UCnet because the “residual” outputs systematically exhibit larger errors (Appendix B.2) and ACnet may be slightly harder to optimize.

In Figure 3b, we compare how much NNs violate enthalpy conservation (RESID) to a related prediction (THERMO), defined as the total thermodynamic tendency in the enthalpy conservation equation:

$$\overbrace{\left( \mathbf{C} \begin{bmatrix} x \\ y_{\text{NN}} \end{bmatrix} \right)}^{\text{RESID}} = \overbrace{\delta p \cdot \left( \dot{T}_{KE} - \dot{T} - \ell_s \dot{q}_v - \ell_f \dot{q}_l \right)}^{\text{THERMO}} + \dots, \quad (13)$$

where the ellipsis includes the surface fluxes, radiation, and precipitation terms. ACnet predicts THERMO more accurately than all NNs by an amount closely related to how much each NN violates enthalpy conservation, followed by LCnet. This yields our second key result: *Enforcing constraints, whether in the architecture or the loss function, can systematically reduce the error of variables related to the constraints.* Since our case has many degrees of freedom, this result does not hold true for individual components of THERMO as their cross-term in equation 9 is larger for ACnet, nor does it hold for variables that are hard to predict deterministically (e.g., precipitation). This motivates physically-constraining a broader class of machine-learning algorithms, such as generative adversarial networks [29, 30]. Finally, note that ACnets can be extended to incorporate inequality constraints on their “direct” outputs (Appendix D), making ACnets applicable to a broad range of constrained optimization problems.

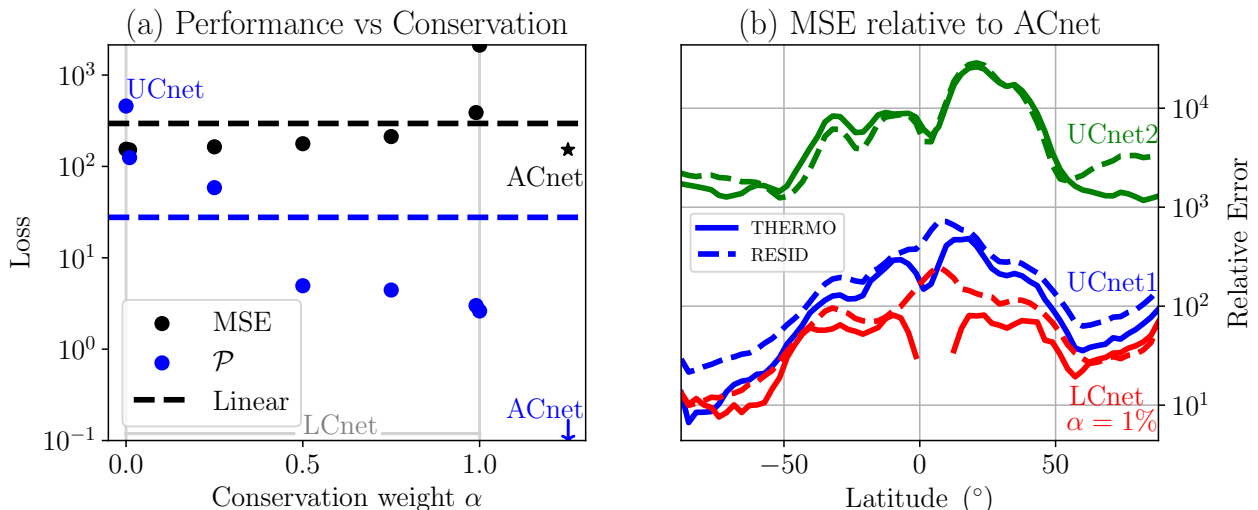


FIG. 3. (a) MSE and  $\mathcal{P}$  averaged over all samples of the validation dataset for UCnet, LCnets of varying  $\alpha$ , and ACnet. The dashed lines indicate MSE and  $\mathcal{P}$  for a multi-linear regression. (b) Mean relative error compared to ACnet in the thermodynamic term (full line) and enthalpy conservation (dotted line) versus latitude.

## ACKNOWLEDGMENTS

Tom Beucler is supported by NSF grants OAC-1835769 and AGS-1734164. We thank Eric Christiansen, Imme Ebert-Uphoff, and Bart Van Merriënboer for advice. We also thank the meteorology department of LMU Munich and the Extreme Science and Engineering Discovery Environment supported by NSF grant number ACI-1548562 (charge numbers TG-ATM190002 and TG-ATM170029) for computational resources.

### A. Derivation of Dimensionless Conservation Equations

The Super-Parametrized Community Atmosphere Model 3.0 embeds a convection-permitting model, namely the System for Atmospheric Modeling [31], in each grid cell of the Community Atmosphere Model 3.0 [32]. In the absence of convective momentum transfer, our convection-permitting model conserves two quantities: liquid/ice water static energy and total water. We recast these conservation equations as an energy (A.1) and mass (A.2) conservation, before adding the conservation of longwave (A.3) and shortwave (A.4) radiation as our network predicts both radiative heating profiles and boundary fluxes at top and bottom of atmosphere, whose difference must match the mass-weighted vertical integral of the heating rate profiles. Finally, we non-dimensionalize all conservation equations in section A.5. We define all variables in Table I.

#### A.1. Conservation of Energy

We define the enthalpy  $H$  of an atmospheric column as the mass-weighted vertical integral of the sum of its sensible heat and latent heat, in  $\text{J m}^{-2}$ , where ice is used as the reference phase of zero energy:

$$H \stackrel{\text{def}}{=} \int_0^{p_s} \frac{dp}{g} \underbrace{(c_p T + L_s q_v + L_f q_l)}_h, \quad (14)$$

where  $p$  is atmospheric pressure in Pa,  $p_s$  is surface pressure in Pa,  $g \approx 9.81 \text{ m s}^{-2}$  is the gravity constant,  $c_p \approx 1.00 \cdot 10^3 \text{ J kg}^{-1} \text{ K}^{-1}$  is the specific heat of water at constant pressure in standard atmospheric conditions,  $T$  is the absolute temperature in K,  $L_s \approx 2.83 \cdot 10^6 \text{ J kg}^{-1}$  is the latent heat of sublimation of water in standard conditions,  $q_v$  is the specific humidity or water vapor mass concentration in kg/kg,  $L_f \approx 3.34 \cdot 10^5 \text{ J kg}^{-1}$  is the latent heat of fusion of water in standard conditions,  $q_l$  is the liquid water mass concentration in kg/kg and  $h$  is the specific enthalpy in  $\text{J kg}^{-1}$ . We isolate the atmospheric column's time-tendency that is due to water phase changes only ( $\Delta_\varphi$ ) for each variable of equation 14:

$$\Delta_\varphi h = -L_f (P - P_i), \quad (15a)$$

$$c_p \Delta_\varphi T = -\text{SHF} + \int_0^{p_s} \frac{dp}{g} c_p (\dot{T} + \dot{T}_{KE}) + \text{SW}_s - \text{SW}_t + \text{LW}_t - \text{LW}_s, \quad (15b)$$

$$L_v \Delta_\varphi q_v = -\text{LHF} + \int_0^{p_s} \frac{dp}{g} L_v \dot{q}_v, \quad (15c)$$

Variable	Name
$\delta p$	Normalized differential pressure reference profile
$\ell_f$	Normalized latent heat of fusion of water
$\ell_s$	Normalized latent heat of sublimation of water
LHF	Latent heat flux
LS	Large-scale forcings in water, temperature, velocity
<b>lw</b>	Longwave heating rate profile
LW <sub>s</sub>	Net surface longwave flux
LW <sub>t</sub>	Net top-of-atmosphere longwave flux
$P$	Total precipitation rate
$P_i$	Solid precipitation rate
$p_s$	Surface pressure
$S_0$	Solar insolation
SHF	Sensible heat flux
<b>sw</b>	Shortwave heating rate profile
SW <sub>s</sub>	Net surface shortwave flux
SW <sub>t</sub>	Net top-of-atmosphere shortwave flux
<b>T</b>	Absolute temperature profile
$\dot{T}$	Convective heating profile
$\dot{T}_{KE}$	Heating from turbulent kinetic energy dissipation
$q_i$	Ice concentration profile
$\dot{q}_i$	Convective ice tendency profile
$q_l$	Liquid water concentration profile
$\dot{q}_l$	Convective liquid water tendency profile
$q_v$	Specific humidity profile
$\dot{q}_v$	Convective water vapor tendency profile
$v$	North-South velocity profile
$z$	Vertical level profile

TABLE I. Definition of Variables: Variables that depend on height are (boldfaced) vectors, referred to as ‘‘profiles’’.

$$\Delta_\varphi q_l = \int_0^{p_s} \frac{dp}{g} \dot{q}_l, \quad (15d)$$

where  $P$  is the total surface precipitation rate in  $\text{kg m}^{-2} \text{s}^{-1}$ ,  $P_i$  is the surface solid precipitation rate in  $\text{kg m}^{-2} \text{s}^{-1}$ , SHF is the surface sensible heat flux in  $\text{W m}^{-2}$ ,  $\dot{T}$  is the time-tendency of temperature in  $\text{K s}^{-1}$ ,  $\dot{T}_{KE}$  is the time-tendency of temperature due to frictional dissipation of kinetic energy in  $\text{K s}^{-1}$ , SW<sub>s</sub> is the net surface downwards shortwave radiative flux in  $\text{W m}^{-2}$ , SW<sub>t</sub> is the net top-of-atmosphere downwards shortwave radiative flux in  $\text{W m}^{-2}$ , LW<sub>t</sub> is the net top-of-atmosphere upwards longwave radiative flux in  $\text{W m}^{-2}$ , LW<sub>s</sub> is the net surface upwards longwave radiative flux in  $\text{W m}^{-2}$ ,  $L_v \approx 2.50 \cdot 10^6 \text{J kg}^{-1}$  is the latent heat of vaporization of water in standard conditions, LHF is the surface latent heat flux in  $\text{W m}^{-2}$ ,  $\dot{q}_v$  is the time tendency of specific humidity in  $\text{kg kg}^{-1} \text{s}^{-1}$  and  $\dot{q}_l$  is the time tendency of liquid water concentration in  $\text{kg kg}^{-1} \text{s}^{-1}$ . We then equate the time-tendencies due to water phase changes in equation 14 to form the equation describing the conservation of column enthalpy:

$$\Delta_\varphi h - c_p \Delta_\varphi T - L_s \Delta_\varphi q_v - L_f \Delta_\varphi q_l = 0. \quad (16)$$

## A.2. Conservation of Mass

The conservation of water states that the change in total column water concentration must balance the sources and sinks of water at the surface, namely the surface evaporation and precipitation rates:

$$\int_0^{p_s} \frac{dp}{g} (\dot{q}_v + \dot{q}_t + \dot{q}_i) = \frac{\text{LHF}}{L_v} - P. \quad (17)$$

## A.3. Conservation of Longwave Radiation

The conservation of longwave radiation states that the difference between the top-of-atmosphere and surface longwave radiative fluxes must balance the net longwave (or longwave) radiative cooling of the atmospheric column to space:

$$\text{LW}_t - \text{LW}_s = - \int_0^{p_s} \frac{dp}{g} c_p \text{lw}, \quad (18)$$

where lw is the vertically-resolved temperature tendency due to longwave heating in  $\text{K s}^{-1}$ .

## A.4. Conservation of Shortwave Radiation

The conservation of shortwave radiation states that the difference between the top-of-atmosphere insolation and the incoming shortwave radiation at the surface must balance the net shortwave radiative heating of the atmospheric column:

$$\text{SW}_t - \text{SW}_s = \int_0^{p_s} \frac{dp}{g} c_p \text{sw}. \quad (19)$$

## A.5. Non-dimensionalization of Conservation Equations

We non-dimensionalize the conservation equations by converting all tendencies to units  $\text{W m}^{-2}$  before dividing them by  $1 \text{W m}^{-2}$ . For numerical modeling purposes, each vertical profile is discretized to 30 vertical levels  $z$  of varying pressure thickness  $\delta \mathcal{P}_z$ . This means that a continuous conservation equations becomes a linear constraint on discrete variables; for instance equation 19 becomes:

$$\text{SW}_t - \text{SW}_s = \sum_{z=1}^{30} \frac{\delta \mathcal{P}_z}{g} c_p \text{sw}_z. \quad (20)$$

To make equation 20 non-dimensional, we introduce a fixed, normalized differential pressure coordinate  $\delta p$  to make the atmospheric pressure  $p$  non-dimensional:

$\forall z, \delta\tilde{p}_z \stackrel{\text{def}}{=} \delta\mathcal{P}_z/\delta p_z$ . This motivates the following non-dimensionalizations:

$$\widetilde{\text{SW}}_t \stackrel{\text{def}}{=} \frac{\text{SW}_t}{1\text{W m}^{-2}} \quad \widetilde{\text{SW}}_s \stackrel{\text{def}}{=} \frac{\text{SW}_s}{1\text{W m}^{-2}} \quad \widetilde{\text{sw}}_z \stackrel{\text{def}}{=} \frac{c_p \delta p_z \text{SW}_z}{g}, \quad (21)$$

which leads to the simpler form of the shortwave conservation equation presented in the main text:

$$\widetilde{\text{SW}}_t - \widetilde{\text{SW}}_s = \sum_{z=1}^{30} \widetilde{\text{sw}}_z \delta\tilde{p}_z = \widetilde{\text{sw}} \cdot \delta\tilde{\mathbf{p}}. \quad (22)$$

For simplicity, the tildes are dropped in the main text and the following appendices.

## B. Implementation of the Architecture-constrained Network

### B.1. Standard Implementation

In our standard implementation, we first output a vector of size  $(218 - 4) = 214$ , before calculating the “residual” component of the output vector by solving the system of equations  $\mathbf{C}[\mathbf{x} \ \mathbf{y}]^T = \mathbf{0}$  from bottom to top and within the network. All layers are implemented in Tensorflow using the functional application programming interface. The first conservation layer (CL<sub>1</sub>) calculates the net shortwave surface flux as a residual of the conservation of shortwave radiation (last row of  $\mathbf{C}$ ):

$$\sum_{i=1}^{30} \text{sw}_z \delta p_z - \text{SW}_t + \text{SW}_s = 0. \quad (23)$$

$$(\text{CL}_1) \quad \underbrace{\text{SW}_s}_{\text{Residual}_4} = \text{SW}_t - \sum_{z=1}^{30} \text{sw}_z \delta p_z. \quad (24a)$$

The second conservation layer (CL<sub>2</sub>) calculates the net longwave surface flux as a residual of the conservation of longwave radiation (third row of  $\mathbf{C}$ ):

$$(\text{CL}_2) \quad \underbrace{\text{LW}_s}_{\text{Residual}_3} = \text{LW}_t - \sum_{z=1}^{30} \text{lw}_z \delta p_z. \quad (24b)$$

The third conservation layer (CL<sub>3</sub>) calculates the lowest-level specific humidity tendency as a residual of the conservation of mass (second row of  $\mathbf{C}$ ):

$$(\text{CL}_3) \quad \delta p_{30} \underbrace{\dot{q}_{v,30}}_{\text{Residual}_2} = \text{LHF} - \text{P} - \sum_{z=1}^{29} \delta p_z \dot{q}_{v,z} - \sum_{z=1}^{30} \delta p_z (\dot{q}_{t,z} + \dot{q}_{i,z}). \quad (24c)$$

The fourth conservation layer (CL<sub>4</sub>) calculates the lowest-level temperature tendency as a residual of the conservation of energy (first row of  $\mathbf{C}$ ):

$$(\text{CL}_4) \quad \delta p_{30} \underbrace{\dot{T}_{30}}_{\text{Residual}_1} = \text{SHF} + \ell_s \text{LHF} + \ell_f (\text{P} - \text{P}_i) - \text{LW}_t + \text{LW}_s + \text{SW}_t - \text{SW}_s - \sum_{z=1}^{29} \delta p_z \dot{T}_z + \sum_{z=1}^{30} \delta p_z \left( \dot{T}_{\text{KE},z} - \ell_s \dot{q}_{v,z} - \ell_f \dot{q}_{t,z} \right). \quad (24d)$$

### B.2. Sensitivity to Residual Index

The indices of the output’s components calculated as “residuals” are hyperparameters of ACnets: While we chose the lowest-level convective heating and moistening tendencies as the “residuals” of our reference ACnet, we are free to choose other vertical levels (e.g., top-of-atmosphere) or other variables (e.g., convective liquid or ice tendencies) as “residuals”. To probe the sensitivity of ACnets to this unfamiliar hyperparameter choice, we train 5 ACnets with different vertical “residual”-levels over 20 epochs, and report their performance and conservation properties in Table II. Each ACnet is referred to as  $q_{z1}T_{z2}$ , where  $z1$  is the index of the “residual” convective moistening for mass conservation, and  $z2$  the index of the “residual” convective heating for energy conservation.

Reassuringly, all ACnets conserve mass, energy and radiation to  $\mathcal{O}(10^{-9}\text{W}^2\text{m}^{-4})$  over both validation datasets. Despite similar baseline skills, ACnet’s mean-performance differs when evaluated in “out-of-training” conditions because of generalization errors at the “residual” vertical level. Figure 4 illustrates these generalization errors by focusing on errors in the convective moistening and heating profiles averaged over the entire validation dataset. Note that averaging the squared-error over the entire validation dataset is equivalent to averaging the squared-error in latitude, longitude, and over the  $\sim 100$ days of our reference simulation. Each ACnet performs worse at its “residual” levels on both validation datasets, with large consequences on the MSE when the errors are large, such as over the (+4K) dataset. For instance,  $q_{14}T_{14}$  (orange line) always produces the largest error at its residual level (horizontal black line) relative to other ACnets. Similarly,  $q_{29}T_{29}$  (green line) and  $q_0T_{29}$  (red line) produce the largest convective heating error at the lowest model level (vertical index 29). Although the sample-to-sample variability is large (e.g., MSE standard deviation in Table II), latitude-pressure and longitude-pressure plots of convective heating and moistening errors show a systematic error increase at the “residual level” (not shown), confirming this is a robust error associated

with the “residual level” hyperparameter. Additional errors in radiative fluxes and precipitation result in the total “out-of-training” MSE, reported on the third row of Table II.

### C. Comparison of Neural Network Types and Architectures

In this section, we distinguish NN types (i.e., LCnet, UCnet, ACnet, see section C.1) from NN architectures (i.e., the standard NN’s hyperparameters, such as number of layers etc., see section C.2). In both cases, we run sensitivity tests to probe the effect of NN’s characteristics on their performance and constraints penalty.

#### C.1 Comparison between LCnets, UCnet and ACnet

The performance and constraints penalties of the different NN types depicted in Figure 3b are compared in Table III:

1. “Linear” is the multi-linear regression baseline, derived by replacing all of UCnet’s leaky rectified linear-unit activations with the identity function.
2. “UCnet 1” is our best-performing NN, i.e. our NN of lowest MSE ( $149W^2m^{-4}$ ). Despite its high performance, it violates conservation laws more than our multi-linear regression, motivating ACnet and LCnet.
3. “UCnet 2” is a poorly-performing NN that we chose because it had the largest difference between constraints penalty and MSE, allowing us to test the consequences of violating conservation laws on prediction abilities.
4. “LCnet ( $\alpha = 0.01$ )” is our LCnet with strictly-positive conservation weight  $\alpha$  of lowest MSE ( $151W^2m^{-4}$ ). The 1% conservation weight is enough to divide the mean penalty of “UCnet 1” by a factor 2.4 over the baseline validation dataset. This improvement does not hold in “out-of-training” conditions, further motivating ACnet.
5. “ACnet” is our reference ACnet described in Appendix B.1. Its MSE is  $152W^2m^{-4}$ , which is only  $3W^2m^{-4}$  more than our lowest-MSE UCnet.

We present the performance and constraints penalties of LCnets of varying conservation weight in Table IV to better characterize the trade-off between performance and physical consistency depicted in Figure 3a. Note that the penalty becomes large as soon as LCnets are evaluated in “out-of-training” conditions, illustrating the limits of enforcing constraints in the loss function.

#### C.2 Sensitivity to Hyperparameters

We conducted a hyperparameter search to address two questions. First, what is the ideal setting of hyperparameters for these experiments? Second, can we better understand the trade-off between performance and constraints?

In order to address the aforementioned questions, we conducted a random search using SHERPA [33], a Python library for hyperparameter tuning. We detail the hyperparameters of interest in Table V, as well as the range of available options during the search. The random search algorithm has the advantage of making no assumptions about the structure of the hyperparameter search problem and is ideal to explore hyperparameter settings. We ran more than 200 trials, each for the full model training of 25 epochs.

We show the hyperparameters of the best-performing unconstrained network in Table VI. The search on networks with  $\alpha = 0$  validated our choice of hyperparameters, as the settings found through exploration are roughly equivalent to those chosen for experiments in this paper (5 layers of 512 nodes, Leaky ReLU coefficient of 0.3, no dropout and no batch normalization). The results notebook can be found at: [https://github.com/jordanott/CBRAIN-CAM/blob/master/notebooks/tbeucler\\_devlog/hp\\_opt\\_conservation/NormalMSE.ipynb](https://github.com/jordanott/CBRAIN-CAM/blob/master/notebooks/tbeucler_devlog/hp_opt_conservation/NormalMSE.ipynb).

In addition to finding promising hyperparameter configurations, the search provided insight into the trade-offs between performance and constraints. For instance, we identified UCnet2, whose hyperparameters are shown in Table VII, as the NN of maximum validation discrepancy between performance (here MSE) and  $\mathcal{P}$ . We then targeted UCnet2 for additional investigations (Figure 3b).

Finally, running a plethora of models helped us choose the number of epochs. Figure 5 shows training and validation MSE curves for more than 200 models. Both metrics plateau after 20 epochs, indicating this is an appropriate time to terminate training.

### D. Enforcing Inequality Constraints in Architecture-Constrained Networks

In this section, we briefly discuss how to enforce inequality constraints in ACnets using a concrete example: the positivity of liquid water concentration in this letter’s NN parametrization of convection. This inequality requires the liquid water concentration  $q_{l,z}(t)$  at a given vertical level  $z$  and at the current timestep  $t$  to be positive. In practice, the liquid water concentration  $q_{l,z}(t)$  is obtained from the liquid water concentration  $q_{l,z}(t-1)$  and the liquid water tendency  $\dot{q}_{l,z}(t-1)$  at the previous timestep  $t-1$  through time-stepping, which means that

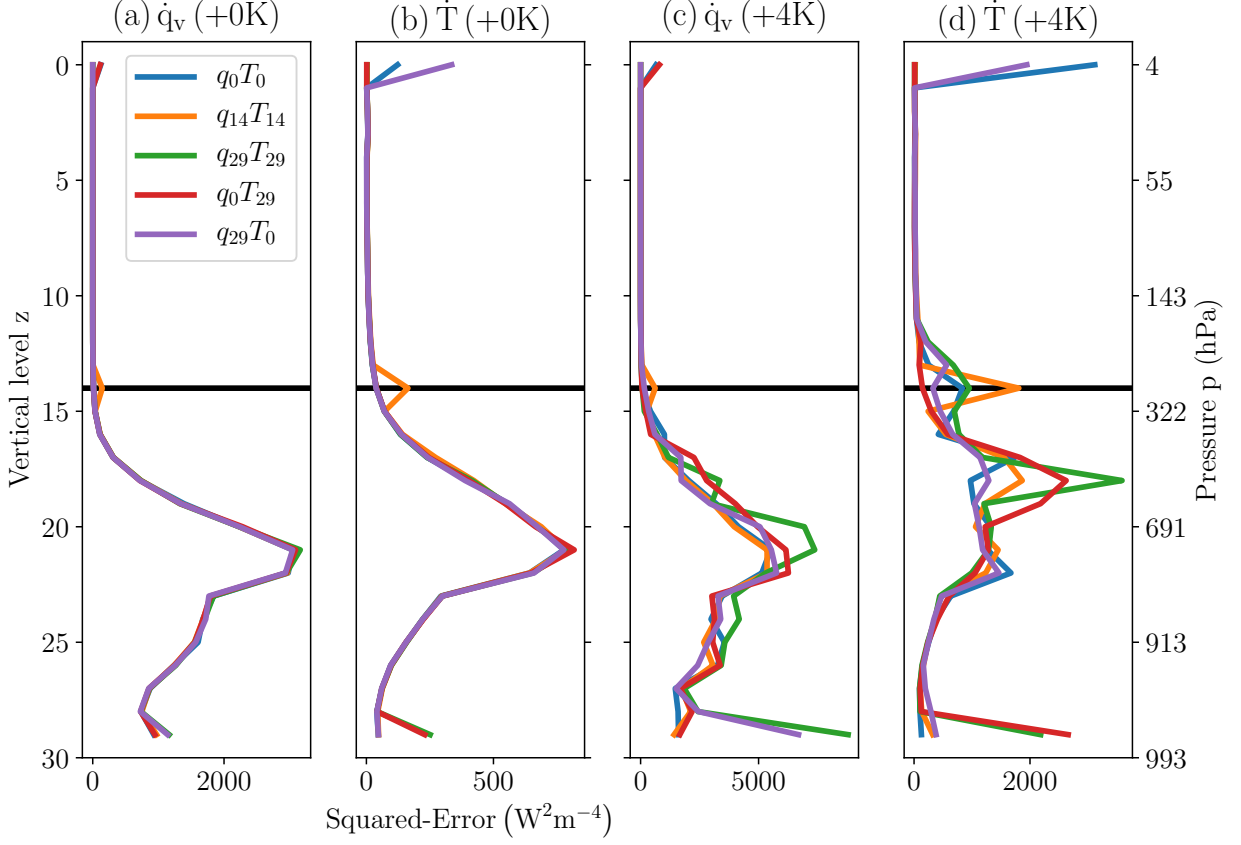


FIG. 4. Squared validation error in convective moistening  $\dot{q}_v$  and heating  $\dot{T}$  versus pressure, for the baseline (+0K) and uniform-warming (+4K) cases. The vertical level of index 0 is at the top of the atmosphere (0hPa), the vertical level of index 14 indicated with a black horizontal line, and the vertical level of index 29 at the surface (1000hPa).

Validation	Metric	$q_0T_0$	$q_{14}T_{14}$	$q_{29}T_{29}$	$q_0T_{29}$	$q_{29}T_0$
Baseline skill (+0K)	MSE	$1.6 \cdot 10^{+02} \pm 9.8 \cdot 10^{+02}$	$1.6 \cdot 10^{+02} \pm 9.9 \cdot 10^{+02}$	$1.6 \cdot 10^{+02} \pm 9.9 \cdot 10^{+02}$	$1.6 \cdot 10^{+02} \pm 9.8 \cdot 10^{+02}$	$1.6 \cdot 10^{+02} \pm 9.8 \cdot 10^{+02}$
	$\mathcal{P}$	$7.8 \cdot 10^{-10} \pm 1.3 \cdot 10^{-09}$	$7.7 \cdot 10^{-10} \pm 1.3 \cdot 10^{-09}$	$8.2 \cdot 10^{-10} \pm 1.4 \cdot 10^{-09}$	$8.0 \cdot 10^{-10} \pm 1.4 \cdot 10^{-09}$	$7.6 \cdot 10^{-10} \pm 1.3 \cdot 10^{-09}$
Uni. warming (+4K)	MSE	$3.8 \cdot 10^{+02} \pm 3.2 \cdot 10^{+03}$	$4.4 \cdot 10^{+02} \pm 6.2 \cdot 10^{+03}$	$4.8 \cdot 10^{+02} \pm 4.6 \cdot 10^{+03}$	$4.8 \cdot 10^{+02} \pm 7.4 \cdot 10^{+03}$	$5.0 \cdot 10^{+02} \pm 6.8 \cdot 10^{+03}$
	$\mathcal{P}$	$1.6 \cdot 10^{-09} \pm 3.8 \cdot 10^{-09}$	$1.1 \cdot 10^{-09} \pm 1.9 \cdot 10^{-09}$	$1.4 \cdot 10^{-09} \pm 2.9 \cdot 10^{-09}$	$1.1 \cdot 10^{-09} \pm 1.8 \cdot 10^{-09}$	$1.3 \cdot 10^{-09} \pm 2.6 \cdot 10^{-09}$

TABLE II. ACnets of varying residual levels for convective moistening (*q*) and heating (*T*) conservation, presented in Figure 4 (Mean MSE/Penalty  $\pm$  Standard deviation over all samples of the validation set)

we can write the positivity constraint as:

$$q_{l,z}(t) = \underbrace{q_{l,z}(t-1)}_{\text{Input}} + \Delta t \times \underbrace{\dot{q}_{l,z}(t-1)}_{\text{Output}} \geq 0, \quad (25)$$

where we note that  $q_{l,z}(t-1)$  is a NN input while  $\dot{q}_{l,z}(t-1)$  is a NN output.

To enforce this inequality constraint in ACnet, we choose  $\dot{q}_{l,z}(t-1)$  to be a “direct” NN output and add an inequality constraints layer (ICL) before the constraints layer (CL). A possible implementation of (ICL) uses the rectified linear unit (ReLU) activation function:

$$\underbrace{\dot{q}_{l,z}(t-1)}_{\text{After (ICL)}} = \text{ReLU} \left[ \underbrace{\dot{q}_{l,z}(t-1) + \Delta t^{-1} q_{l,z}(t-1)}_{\text{Before (ICL)}} - \Delta t^{-1} q_{l,z}(t-1) \right], \quad (26)$$

Validation	Metric	Linear	UC <sub>net</sub> 1	UC <sub>net</sub> 2	LC <sub>net</sub> ( $\alpha = 0.01$ )	AC <sub>net</sub>
Baseline skill (+0K)	MSE	$3.0 \cdot 10^{+02} \pm 1.7 \cdot 10^{+03}$	$1.5 \cdot 10^{+02} \pm 9.4 \cdot 10^{+02}$	$3.4 \cdot 10^{+02} \pm 2.2 \cdot 10^{+03}$	$1.5 \cdot 10^{+02} \pm 9.5 \cdot 10^{+02}$	$1.5 \cdot 10^{+02} \pm 9.6 \cdot 10^{+02}$
	$\mathcal{P}$	$2.8 \cdot 10^{+01} \pm 2.3 \cdot 10^{+01}$	$9.1 \cdot 10^{+01} \pm 8.2 \cdot 10^{+01}$	$2.9 \cdot 10^{+03} \pm 3.4 \cdot 10^{+03}$	$3.8 \cdot 10^{+01} \pm 2.8 \cdot 10^{+01}$	$7.7 \cdot 10^{-10} \pm 1.4 \cdot 10^{-09}$
Uni. warming (+4K)	MSE	$7.5 \cdot 10^{+02} \pm 1.3 \cdot 10^{+04}$	$3.5 \cdot 10^{+02} \pm 3.6 \cdot 10^{+03}$	$4.5 \cdot 10^{+02} \pm 2.6 \cdot 10^{+03}$	$3.7 \cdot 10^{+02} \pm 4.2 \cdot 10^{+03}$	$3.6 \cdot 10^{+02} \pm 4.3 \cdot 10^{+03}$
	$\mathcal{P}$	$2.6 \cdot 10^{+02} \pm 1.8 \cdot 10^{+03}$	$2.7 \cdot 10^{+02} \pm 5.6 \cdot 10^{+02}$	$4.0 \cdot 10^{+03} \pm 5.4 \cdot 10^{+03}$	$2.5 \cdot 10^{+02} \pm 7.3 \cdot 10^{+02}$	$1.4 \cdot 10^{-09} \pm 2.9 \cdot 10^{-09}$

TABLE III. NN presented in Figure 3b (Mean MSE/Penalty  $\pm$  Standard deviation over all samples of the validation set)

Validation	Metric	UC <sub>net</sub> ( $\alpha = 0$ )	$\alpha = 0.25$	$\alpha = 0.5$	$\alpha = 0.75$	$\alpha = 0.99$
Baseline skill (+0K)	MSE	$1.5 \cdot 10^{+02} \pm 1.6 \cdot 10^{+03}$	$1.6 \cdot 10^{+02} \pm 1.0 \cdot 10^{+03}$	$1.8 \cdot 10^{+02} \pm 1.1 \cdot 10^{+03}$	$2.1 \cdot 10^{+02} \pm 1.2 \cdot 10^{+03}$	$3.9 \cdot 10^{+02} \pm 1.8 \cdot 10^{+03}$
	$\mathcal{P}$	$4.6 \cdot 10^{+02} \pm 4.7 \cdot 10^{+02}$	$5.9 \cdot 10^{+01} \pm 6.4 \cdot 10^{+01}$	$4.9 \cdot 10^{+00} \pm 4.9 \cdot 10^{+00}$	$4.4 \cdot 10^{+00} \pm 2.7 \cdot 10^{+00}$	$3.0 \cdot 10^{+00} \pm 1.9 \cdot 10^{+00}$
Uni. warming (+4K)	MSE	$6.3 \cdot 10^{+02} \pm 7.1 \cdot 10^{+03}$	$4.9 \cdot 10^{+02} \pm 9.0 \cdot 10^{+03}$	$5.0 \cdot 10^{+02} \pm 7.6 \cdot 10^{+03}$	$7.6 \cdot 10^{+02} \pm 1.4 \cdot 10^{+04}$	$6.3 \cdot 10^{+02} \pm 3.5 \cdot 10^{+03}$
	$\mathcal{P}$	$2.6 \cdot 10^{+04} \pm 1.1 \cdot 10^{+05}$	$4.8 \cdot 10^{+02} \pm 1.9 \cdot 10^{+03}$	$4.7 \cdot 10^{+02} \pm 2.2 \cdot 10^{+03}$	$9.6 \cdot 10^{+01} \pm 3.5 \cdot 10^{+02}$	$4.2 \cdot 10^{+02} \pm 1.3 \cdot 10^{+03}$

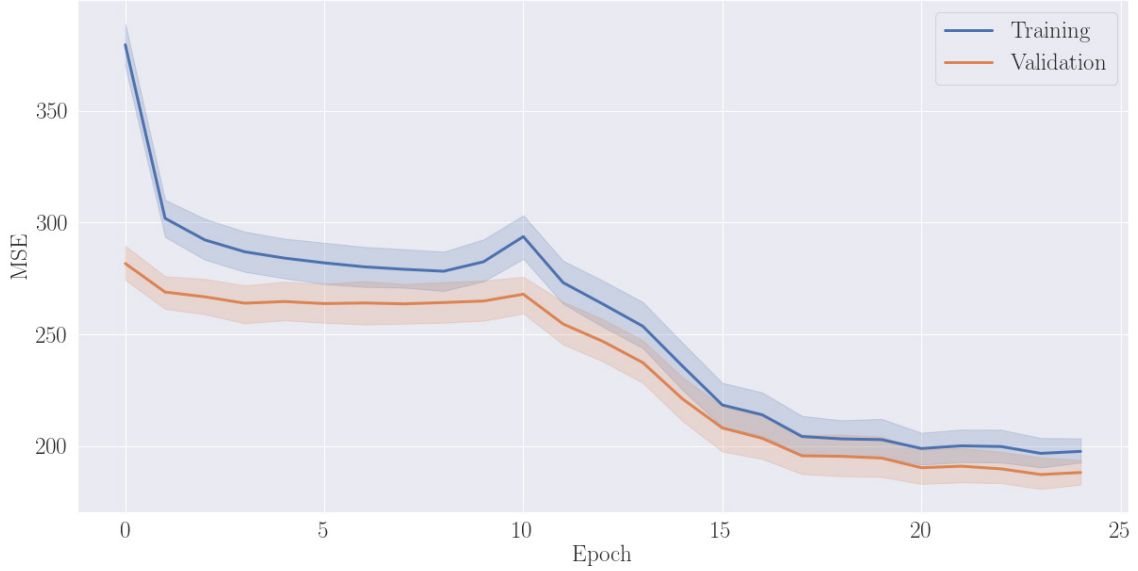
TABLE IV. LCnets of varying weight  $\alpha$ , presented in Figure 3a (Mean MSE/Penalty  $\pm$  Standard deviation over all samples of the validation set)

FIG. 5. Training MSE and Validation MSE over time from more than 200 models.

TABLE V. Hyperparameter Space

Name	Options	Parameter Type
Batch Normalization	[yes, no]	Choice
Dropout	[0, 0.25]	Continuous
Leaky ReLU coefficient	[0 - 0.4]	Continuous
Learning Rate	[0.0001 - 0.01]	Continuous (log)
Nodes per Layer	[400 - 600]	Discrete
Number of layers	[3 - 8]	Discrete

TABLE VI. Best hyperparameter configuration for  $\alpha = 0$ 

Batch Normalization	No
Dropout	0.00975
Leaky ReLU coefficient	0.25373
Learning Rate	0.000977
Number of layers	5
Nodes per Layer	[625, 517, 543, 538, 692]

TABLE VII. Hyperparameter configuration for UCnet2

Batch Normalization	Yes
Dropout	0.246414
Leaky ReLU coefficient	0.007623
Learning Rate	0.000641
Number of layers	7
Nodes per Layer	[328, 558, 680, 387, 648, 518, 538 ]

so that the liquid water tendency after (ICL) yields a positive liquid water concentration  $q_{l,z}(t)$  at the current timestep. Since the inequality constraints layer (ICL) comes before the constraints layer, we can still enforce the equality constraints ( $\mathcal{C}$ ) to machine precision. Fi-

nally, note that the previous example can be generalized to non-linear analytic constraints involving less than ( $p$ - $n$ ) inputs, allowing ACnets to enforce a broad range of inequality constraints.

- 
- [1] M. Reichstein, G. Camps-Valls, B. Stevens, M. Jung, J. Denzler, N. Carvalhais, and Prabhat, Deep learning and process understanding for data-driven Earth system science, *Nature* **566**, 195 (2019).
- [2] K. J. Bergen, P. A. Johnson, M. V. De Hoop, and G. C. Beroza, Machine learning for data-driven discovery in solid Earth geoscience (2019).
- [3] A. Karpatne, G. Atluri, J. H. Faghmous, M. Steinbach, A. Banerjee, A. Ganguly, S. Shekhar, N. Samatova, and V. Kumar, Theory-guided data science: A new paradigm for scientific discovery from data, *IEEE Transactions on Knowledge and Data Engineering* **29**, 2318 (2017).
- [4] P. Márquez-Neila, M. Salzmann, and P. Fua, Imposing Hard Constraints on Deep Networks: Promises and Limitations, (2017), arXiv:1706.02025.
- [5] M. Raissi, P. Perdikaris, and G. E. Karniadakis, Physics Informed Deep Learning (Part I): Data-driven Solutions of Nonlinear Partial Differential Equations, (2017), arXiv:1711.10561.
- [6] Y. Bar-Sinai, S. Hoyer, J. Hickey, and M. P. Brenner, Learning data-driven discretizations for partial differential equations, *Proceedings of the National Academy of Sciences* **116**, 15344 (2019).
- [7] E. de Bezenac, A. Pajot, and P. Gallinari, Deep Learning for Physical Processes: Incorporating Prior Scientific Knowledge, (2017), arXiv:1711.07970.
- [8] J. Ling, A. Kurzawski, and J. Templeton, Reynolds averaged turbulence modelling using deep neural networks with embedded invariance, *Journal of Fluid Mechanics* **807**, 155 (2016).
- [9] J. L. Wu, H. Xiao, and E. Paterson, Physics-informed machine learning approach for augmenting turbulence models: A comprehensive framework, *Physical Review Fluids* **7**, 074602 (2018).
- [10] A. Karpatne, W. Watkins, J. Read, and V. Kumar, Physics-guided Neural Networks (PGNN): An Application in Lake Temperature Modeling, (2017), arXiv:1710.11431.
- [11] X. Jia, J. Willard, A. Karpatne, J. Read, J. Zwart, M. Steinbach, and V. Kumar, Physics guided RNNs for modeling dynamical systems: A case study in simulating lake temperature profiles, in *SIAM International Conference on Data Mining, SDM 2019* (2019) pp. 558–566, arXiv:1810.13075v2.
- [12] T. Beucler, S. Rasp, M. Pritchard, and P. Gentine, Achieving Conservation of Energy in Neural Network Emulators for Climate Modeling, (2019), arXiv:1906.06622.
- [13] A. K. Jain, J. Mao, and K. M. Mohiuddin, Artificial neural networks: A tutorial (1996).
- [14] M. W. Gardner and S. R. Dorling, Artificial neural networks (the multilayer perceptron) - a review of applications in the atmospheric sciences, *Atmospheric Environment* **32**, 2627 (1998).
- [15] T. Palmer, G. Shutts, R. Hagedorn, F. Doblas-Reyes, T. Jung, and M. Leutbecher, Representing Model Uncertainty in Weather and Climate Prediction, *Annual Review of Earth and Planetary Sciences* **33**, 163 (2005).
- [16] T. Schneider, J. Teixeira, C. S. Bretherton, F. Brient, K. G. Pressel, C. Schär, and A. P. Siebesma, Climate goals and computing the future of clouds, *Nature Climate Change* **7**, 3 (2017).
- [17] V. M. Krasnopolsky, M. S. Fox-Rabinovitz, and A. A. Belochitski, Using Ensemble of Neural Networks to Learn Stochastic Convection Parameterizations for Climate and Numerical Weather Prediction Models from Data Simulated by a Cloud Resolving Model, *Advances in Artificial Neural Systems* **2013**, 1 (2013).
- [18] S. Rasp, M. S. Pritchard, and P. Gentine, Deep learning to represent sub-grid processes in climate models, *Proceedings of the National Academy of Sciences of the United States of America* **115**, 9684 (2018), arXiv:1806.04731.
- [19] N. D. Brenowitz and C. S. Bretherton, Prognostic Validation of a Neural Network Unified Physics Parameterization, *Geophysical Research Letters* **45**, 6289 (2018).
- [20] P. A. O’Gorman and J. G. Dwyer, Using Machine Learning to Parameterize Moist Convection: Potential for Modeling of Climate, Climate Change, and Extreme Events (2018).
- [21] S. Rasp, Online learning as a way to tackle instabilities and biases in neural network parameterizations, (2019), arXiv:1907.01351.
- [22] M. Khairoutdinov, D. Randall, and C. DeMott, Simulations of the Atmospheric General Circulation Using a Cloud-Resolving Model as a Superparameterization of

- Physical Processes, *Journal of the Atmospheric Sciences* **62**, 2136 (2005).
- [23] M. S. Pritchard, C. S. Bretherton, and C. A. Demott, Restricting 32-128 km horizontal scales hardly affects the MJO in the Superparameterized Community Atmosphere Model v.3.0 but the number of cloud-resolving grid columns constrains vertical mixing, *Journal of Advances in Modeling Earth Systems* **6**, 723 (2014).
- [24] J. A. Andersen and Z. Kuang, Moist static energy budget of MJO-like disturbances in the atmosphere of a zonally symmetric aquaplanet, *Journal of Climate* **25**, 2782 (2012).
- [25] F. Chollet, Keras (2015).
- [26] M. Abadi, A. Agarwal, P. Barham, E. Brevdo, Z. Chen, C. Citro, G. S. Corrado, A. Davis, J. Dean, M. Devin, S. Ghemawat, I. Goodfellow, A. Harp, G. Irving, M. Isard, Y. Jia, R. Jozefowicz, L. Kaiser, M. Kudlur, J. Levenberg, D. Mane, R. Monga, S. Moore, D. Murray, C. Olah, M. Schuster, J. Shlens, B. Steiner, I. Sutskever, K. Talwar, P. Tucker, V. Vanhoucke, V. Vasudevan, F. Viegas, O. Vinyals, P. Warden, M. Wattenberg, M. Wicke, Y. Yu, and X. Zheng, TensorFlow: Large-Scale Machine Learning on Heterogeneous Distributed Systems, (2016), arXiv:1603.04467.
- [27] T. Tieleman, G. E. Hinton, N. Srivastava, and K. Swersky, Lecture 6.5-rmsprop: Divide the gradient by a running average of its recent magnitude, COURSERA: Neural Networks for Machine Learning **4**, 26 (2012).
- [28] D. P. Kingma and J. Ba, Adam: A Method for Stochastic Optimization, (2014), arXiv:1412.6980.
- [29] J.-L. Wu, K. Kashinath, A. Albert, D. Chirila, Prabhath, and H. Xiao, Enforcing Statistical Constraints in Generative Adversarial Networks for Modeling Chaotic Dynamical Systems, (2019), arXiv:1905.06841.
- [30] I. Goodfellow, J. Pouget-Abadie, M. Mirza, B. Xu, D. Warde-Farley, S. Ozair, A. Courville, Y. Bengio, and Y. Y. Wang, Generative Adversarial Nets, in *Proceedings of the Annual Conference of the International Speech Communication Association, INTERSPEECH*, Vol. 08-12-Sept (2016) pp. 715–719, arXiv:1406.2661v1.
- [31] M. F. Khairoutdinov and D. a. Randall, Cloud Resolving Modeling of the ARM Summer 1997 IOP: Model Formulation, Results, Uncertainties, and Sensitivities, *Journal of the Atmospheric Sciences* **60**, 607 (2003).
- [32] W. D. Collins, P. J. Rasch, B. A. Boville, J. J. Hack, J. R. McCaa, D. L. Williamson, B. P. Briegleb, C. M. Bitz, S. J. Lin, and M. Zhang, The formulation and atmospheric simulation of the Community Atmosphere Model version 3 (CAM3), *Journal of Climate* **19**, 2144 (2006).
- [33] L. Hertel, P. Sadowski, J. Collado, and P. Baldi, Sherpa : Hyperparameter Optimization for Machine Learning Models, *Conference on Neural Information Processing Systems (NIPS)* (2018).